What drove the Stony Coral Tissue Loss Disease outbreak in Florida ?

Thomas Dobbelaere [1,*], **Erinn Muller** [2], **Lewis Gramer** [3,4], **Dan Holstein** [5] **and Emmanuel Hanert** [1,6]

[1] *Earth and Life Institute (ELI), UCLouvain, Louvain-la-Neuve, Belgium*

[2] *Coral Health and Disease Program, Mote Marine Laboratory, Sarasota, FL, USA*

[3] *Cooperative Institute for Marine and Atmospheric Studies (CIMAS), University of Miami, Miami, FL, USA*

[4] *Atlantic Oceanographic and Meteorological Laboratory (AOML), NOAA, Miami, FL, USA*

[5] *Department of Oceanography and Coastal Sciences, College of the Coast and Environment, Louisiana State University, Baton Rouge, LA, USA*

[6] *Institute of Mechanics, Materials and Civil Engineering (IMMC), UCLouvain, Louvain-la-Neuve, Belgium*

Correspondence*:
Earth and Life Institute (ELI), UCLouvain, Croix du Sud 2 box L7.05.16, B-1348 Louvain-la-Neuve, Belgium
thomas.dobbelaere@uclouvain.be

2 ABSTRACT

For about six years, the Florida Reef Tract (FRT) has been experiencing an outbreak of the Stony Coral Tissue Loss Disease (SCTLD). First reported off the coast of Miami-Dade County in 2014, the SCTLD has since spread throughout the entire FRT with the exception of the Dry Tortugas. However, the causative agent for this outbreak is currently unknown. Here we show how a high-resolution bio-physical model with a modified patch SIR epidemic model can inform on the potential characteristics of the causative agent of the disease and its vector. In this study, the agent is assumed to be transported within composite material (such as coral mucus, dying tissues and/or resuspended sediments) driven by currents and potentially persisting in the water column for extended periods of time. In this framework, our simulations suggest that the SCTLD is likely to be propagated within neutrally buoyant materials driven by mean barotropic currents. Calibration of our model parameters with field data show that corals are then infected within a mean transmission time of 6.45 days. Furthermore, the propagation speed of the disease through the FRT is shown to be very sensitive to the value of an infection threshold, defined the proportion of infectious corals that causes an exponential growth of the disease on the colony. Our results present a new connectivity-based approach to understand the spread of the SCTLD through the FRT. Such method can provide a valuable complement to field observations and lab experiments to support the management of the epidemic as well as the identification of its causative agent.

Keywords: stony-coral-tissue-loss disease, biophysical modeling, Florida reef tract, spatial epidemiology, connectivity

1 INTRODUCTION

Coral diseases are a major threat to coral reef ecosystems and have led to significant declines in coral cover especially within the Caribbean region (Richardson et al., 1998; Sutherland et al., 2004; Aronson and

23 Precht, 2001; Harvell et al., 2007; Miller et al., 2009; Brandt and McManus, 2009). Indeed, the Florida
24 reef tract, which was dominated by Acropora palmata and Acropora cervicornis, and often had 30% coral
25 cover until the 1970s/80s (Dustan and Halas, 1987; Porter and Meier, 1992), is now dominated by bare
26 substrate, octocorals, and macroalgae with only approximately 5% stony coral cover remaining (Ruzicka
27 et al., 2013). The loss of the branching Acroporid species was attributed primarily to a disease outbreak,
28 termed white band disease (Aronson and Precht, 2001), but several other threats such as habitat reduction,
29 eutrophication, overfishing, hurricanes, and bleaching likely all contributed to these species decline (Team,
30 2005). Subsequent losses of coral cover within the region were often linked to additional disease incidences
31 and repeated regional coral bleaching events as a result of global climate change (Kuta and Richardson,
32 1996; Richardson et al., 1998; Sutherland et al., 2004; Gardner et al., 2003; Aronson and Precht, 2006;
33 Kuffner et al., 2015; Manzello, 2015). A novel coral disease outbreak, termed Stony Coral Tissue Loss
34 Disease (SCTLD), is now threatening the last vestiges of coral throughout the Florida reef tract.

35   SCTLD was first documented off the coast of Miami-Dade County in the summer of 2014 by Precht
36 et al. (2016) and has since spread throughout the entire Florida reef tract with the exception of the Dry
37 Tortugas. To date, SCTLD has been observed affecting over 20 different stony corals species. A case
38 definition of SCTLD has been compiled to describe the visual appearance and ecology of SCTLD (NOAA,
39 2018). Briefly, the gross morphology of SCTLD is described as focal or multifocal, with locally extensive
40 to diffuse areas of acute to subacute tissue loss distributed basally, peripherally, or both. In some cases,
41 tissues bordering areas of chronic tissue loss show indistinct bands (1–5 cm) of pallor, progressing to
42 normal pigmentation away from the denuded skeleton. There is also a range in coral susceptibility to
43 SCTLD, with species categorized as highly susceptible (e.g., Dendrogyra cylindrus, Dichocoenia stokesii,
44 Meandrina meandrites), moderately susceptible (e.g., Orbicella spp., Montastraea cavernosa, Siderastrea
45 siderea, Stephanocoenia intersepta), or tolerant (e.g., Porites spp., Acropora spp.). Unfortunately, SCTLD
46 has not remained isolated in the Florida reef tract and has now been recorded in Mexico (Alvarez-Filip
47 et al., 2019), the USVI (Blondeau et al., 2020) and several other locations around the Caribbean (Kramer
48 et al., 2019). The continued persistence of the outbreak, the high number of species affected, and the large
49 geographical range of reports consistent with the case definition suggests that SCTLD is the largest coral
50 disease outbreak on record

51   Large-scale spatial epidemiologic analyses showed that the reefs in Florida with SCTLD are clustered,
52 supporting a contagious mode of transmission (Muller et al., 2020). Similarly, aquaria-based experiments
53 indicate SCTLD can be transmitted through direct contact or indirectly through the water column (Aeby
54 et al., 2019) suggesting water can be a SCTLD vector, at least within a controlled setting. The initial
55 exponential increase in spread among reefs from the disease epicenter (Precht et al., 2016) and the persistent
56 subsequent linear rate of spread of SCTLD (Muller et al., 2020), north along South Florida reefs and south
57 into the Florida Keys, indicates that water currents may play a role in disease transmission. Furthermore,
58 the rate of spread, estimated at 100 m per day, suggests surface currents are likely too fast to have spread
59 SCTLD within the region. These results imply that the bottom boundary layer, which is significantly
60 slower than surface currents, may be the vertical location in which transmission occurs (Aeby et al.,
61 2019). However, to date, there have been no efforts linking local hydrodynamic modeling efforts with the
62 spatio-temporal dynamics of SCTLD in Florida.

63   Estimating the transport of infectious material from reef to reef by currents cannot be performed
64 empirically. However, experimentally-calibrated numerical models that simulate currents can provide a
65 realistic picture of the dispersal of disease agents. Nonetheless, accurately modeling water circulation at
66 the spatial scales that affect this dispersal remains a key challenge, as small-scale flow features such as

67 recirculation eddies around reefs and islands strongly impact exchanges between reefs (Wolanski, 1994;
68 Burgess et al., 2007; Figueiredo et al., 2013). In this context, models that can explicitly simulate flow
69 features down to the reef scale are needed. This represents a spatial resolution of the order of 100-1,000 m
70 in dense reef systems. As of today, most regional ocean models using traditional numerical methods cannot
71 achieve such resolution because of the computational resources it requires. To our knowledge, the best
72 resolution currently available among these models in the FRT is $\sim$ 900 m with the FKEYS-HYCOM model
73 that has been developed for the Florida Keys region (Kourafalou and Kang, 2012; Sponaugle et al., 2012;
74 Vaz et al., 2016). Unstructured-mesh ocean models offer a potential solution to this resolution issue by
75 locally increasing the model resolution close to reefs and islands (Lambrechts et al., 2008; Thomas et al.,
76 2014, 2015), in order to focus the computational resources where they are most needed. High resolution
77 bio-physical dispersal models can be used to build the potential connectivity between reefs and therefore
78 approximate exchanges between colonies in the complex topography of the coral reef systems (Frys et al.,
79 2020).

80 Marine diseases differ significantly from better studied terrestrial diseases, namely due to the potential for
81 long environmental residence times, during which pathogens may survive and disperse through the water
82 (Harvell et al., 2007; Sokolow, 2009). Several recent studies have attempted to adapt traditional epidemic
83 models (Susceptible-Infectious-Recovered, or SIR models) to coral reef systems (Sokolow, 2009; Bidegain
84 et al., 2016a,b). Novel approaches have included developing pathogen pools (Bidegain et al., 2016a,b),
85 and to model at the metapopulation scale, rather than at the scale of coral holobionts (Sokolow, 2009).
86 Both of these approaches are attempting to address the same issue: Infection occurs between patches of
87 entirely sessile animals, through the dispersal of pathogen(s). Thus, there are internal within-patch disease
88 dynamics and metapopulation-scale between-patch dynamics occurring simultaneously. The epidemic
89 model developed in this study utilizes the same basic architecture of previous coral reef SIR models, but
90 rather than assume pathogen pools (e.g. Bidegain et al. (2016a,b)) or ignore internal patch dynamics (e.g.
91 Sokolow (2009)), we have modeled both within-patch disease dynamics and the dispersal of pathogens
92 explicitly using potential connectivity networks.

93 The objective of this study was to deduce the probable propagation mechanism of the SCTLD throughout
94 the FRT by developing an experimentally-calibrated epidemio-hydrodynamic model. With a resolution of
95 about 100 m, this model can capture potential exchanges of disease-carrying matter, further denominated
96 as "infectious" in our modeling framework, between reefs that would be ignored by coarser models. By
97 reproducing the observed spread of disease between 1st May 2018 and 1st April 2014, we provide insight
98 on the characteristics of the disease agent and its vector. Ultimately, our model, coupled with lab and field
99 works, would support the management of the epidemic and the identification of its causative agent.

2 METHODS

2.1 Modeling reef connectivity

101 In this study, we focus on the exchanges of infectious material between coral reefs driven by ocean
102 currents, which therefore have to be accurately simulated. An ocean model should provide a realistic
103 large-scale circulation while also resolving small-scale flow features down to the scale of individual reefs.
104 In this study, we use the unstructured-mesh depth-integrated coastal ocean model SLIM[1] to simulate ocean
105 currents over an area that includes the FRT but also the Florida Strait and part of the Gulf of Mexico (Fig.
106 1). By using an unstructured mesh, we can increase the model resolution only over the FRT and hence
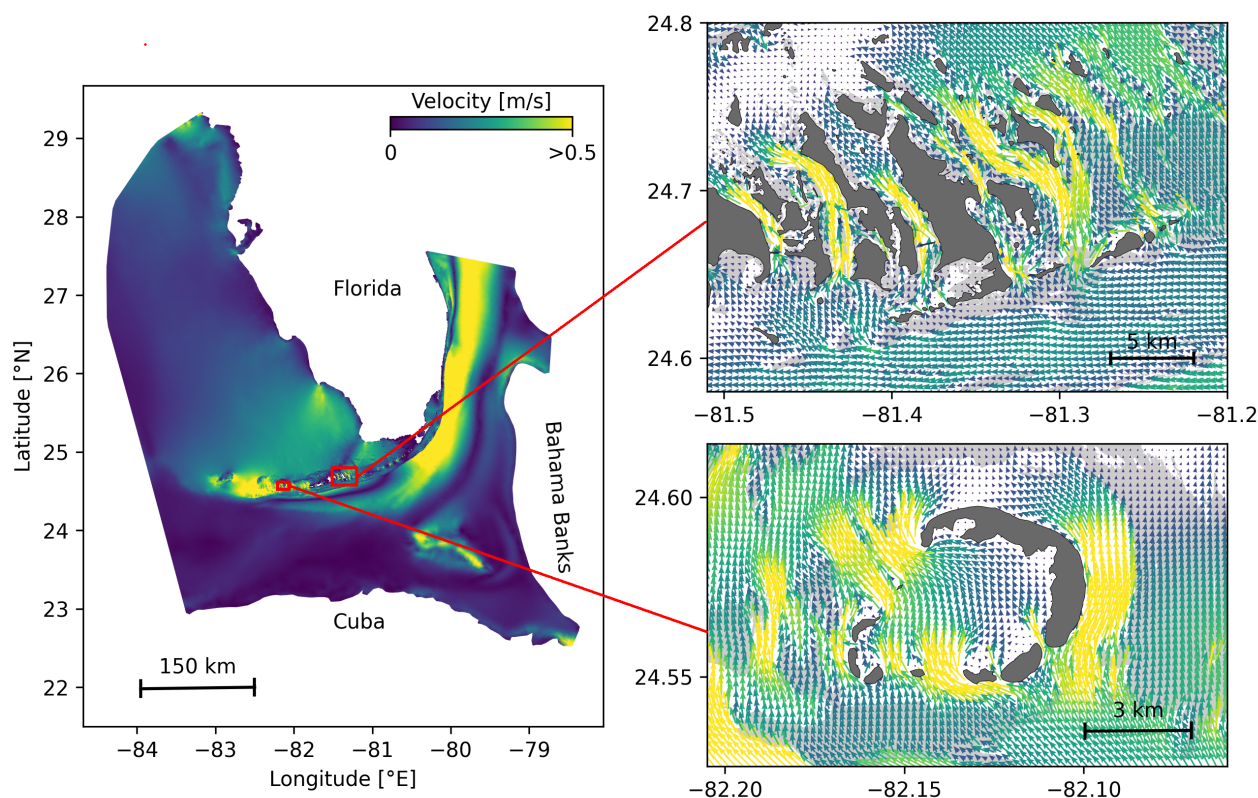
---

[1] `https://www.slim-ocean.be`

Figure 1. Model computational domain and close-up views of the mesh with snapshots of the currents on May, 25 2018 at 00:00, for the Marquesas Keys (bottom) and the Lower Keys (top). This illustrates the benefits of unstructured meshes to represent the fine-scale details of the topography and hence simulate currents down to the scale of individual reefs (shown in light grey) and islands (shown in darker grey).

107 concentrate computational resources where they are most needed. SLIM , being a depth-averaged model, is
108 well suited to shallow-water flows. Details of the model formulation and validation are provided in Frys
109 et al. (2020).

110   The mesh resolution depends only on the distance to the coast, but we distinguish between the coastlines
111 along the FRT where we impose a maximum resolution of 100 m and the other coastlines along which
112 the maximum resolution is 2500 m. The mesh has been generated with the open-source mesh generator
113 GMSH (Geuzaine and Remacle, 2009) and has about 7×10^5 elements. The coarsest elements, far away
114 from the FRT, have a size of about 10 km. An illustration of ocean currents simulated on that mesh are
115 shown in Fig. 1. It shows how a 100-m spatial resolution allows us to simulate fine-scale details of the flow,
116 such as recirculation eddies and currents within the dense reef system in the Lower Keys that consist of
117 many individual reefs with narrow passages in between.

118   The simulated currents can then be used to model dispersal of infectious material throughout the FRT.
119 In this study, 3 types of potential vector carrying the disease causative agent were considered: positively
120 buoyant (e.g. mucus and surfactant), neutrally buoyant (e.g. fines, pelagic organisms) and negatively
121 buoyant (e.g. sediments, composites, demersal organisms). As SLIM is a depth-averaged model, the
122 mean currents it generates are well suited to model the dispersal of neutrally buoyant material remaining
123 within the water column. However, these currents must be modified to correctly represent the dynamics of
124 materials evolving in the surface and bottom boundary layers. Therefore, surface current response to winds
125 is estimated by adding 1.5% of the wind speed to SLIM currents with a stress-layer veering angle of 45° to

126 the right for positively buoyant particles. Such parametrization is shown to be an accurate approximation
127 of wave-induced Stokes drift and quasi-Eulerian surface currents by (Ardhuin et al., 2009). For negatively
128 buoyant materials, on the other hand, bottom currents are obtained by taking 60% of SLIM currents velocity
129 with a veering angle of $15°$ to the left. This is an approximation based on observations of bottom currents
130 and whole water column current profiles in the shallow waters (<15 m) of Hawk Channel in the middle
131 Florida Keys by Smith (2009), as well as observations obtained during the Atlantic Ocean Acidification
132 Testbed project (Gramer pers. comm.). It is also consistent with the theory of current veering in the bottom
133 Ekman layer, albeit that has previously observed in deeper (30-90 m) coastal waters, e.g., by Perlin et al.
134 (2007) and Kundu (1976).

135   Using these three velocity fields, virtual particles are then released on all the reefs composing the FRT to
136 model the dispersal of infected materials carrying the disease causative agent. The locations of the reefs of
137 Florida are extracted from the "coral reefs and hardbottom" layer of the Unified Florida Reef Tract Map
138 (FWC, 2017). The polygon of this reef map are then further divided into 500 m squares in order to track the
139 propagation of the disease with a finer geographical resolution, generating a total of 16823 polygons. At
140 the beginning of each simulated months and for each type of currents, a total of about 1.5×10^6 particles
141 are released over all the reef polygons. These particles have a state composed of their polygon of origin
142 as well as their mass, initialized to 1, that they loose at a constant rate γ as they are moved by surface,
143 mean or bottom currents. In this study, the value of γ is chosen so that particles have a half life of 30
144 days. When the particles are brought over reef polygons by currents, the amount of infected mass that
145 lands on the polygon is recorded in monthly potential connectivity matrices whose entries are denoted
146 C_{ij}. The matrix rows correspond to the source reefs and the columns correspond to the destination reefs.
147 Hence C_{ij} represents the mass of infected material originating from sub-reef i that has settled on sub-reef j.
148 This matrix is then normalized by dividing each of its rows i by the the total mass of particles released on
149 polygon i in order to obtained the normalized potential connectivity matrix $\tilde{C}$, whose entry $\tilde{C}_{ij}$ gives the
150 probability that infectious material produced on sub-reef i settles on sub-reef j. Connectivity matrices are
151 computed for each type of current and for each month of the simulated period.

152   These connectivity matrices can be more easily handled by interpreting them as large graphs whose
153 vertices are reefs. They can then be analyzed using graph theory tools. In this study, four potential
154 connectivity measures are used to interpret the monthly computed graphs. These indicators are described
155 in Table 1. The first indicator is the weighted connectivity length (WCL), that gives the average dispersal
156 distance from origin to destination for material produced on a given reef. The weighted connectivity of reef
157 polygon i writes:

$$WCL_i = \frac{\sum_j \tilde{C}_{ij} L_{ij}}{\sum_j \tilde{C}_{ij}} \tag{1}$$

158 where L_{ij} is the distance between origin reef i and destination reef j. Another measure of the spreading
159 potential of reef j is its out-degree, *i.e.* the product of the number of connections originating from reef j
160 by the quantity of infectious matter its sends to the network. This indicator is obtained by computing the
161 number non-zero entries of row i of the potential connectivity matrix C and multiplying it with $\sum_j C_{ij}$. The
162 information given by the out-degree is complemented by the proportion of infectious elements produced
163 on reef i that successfully settles on a reef, called the fraction exchanged of reef i. This indicator is
164 given by $\sum_j \tilde{C}_{ij}$. Finally, the isolation of reef i in the network is given by the self recruitment, *i.e.* the
165 proportion of infectious matter settling on reef i that originates from reef i, computed by $C_{ii}/\sum_j C_{ji}$. A
166 large self-recruitment value indicates that few infectious matter produced elsewhere settles on the reef and
167 thus that it is isolated from the rest of the network.

Indicators	Description	What it shows
Weighted connectivity length (WCL)	Average dispersal distance from origin to destination reef for all infectious elements released over a reef	Average distance at which a reef can send infectious matter
Out-degree	Number of out-going connections originating from a given reef multiplied by the total mass exchanged	Potential for a reef to spread the disease
Fraction exchanged	Fraction of infectious material produced on a given reef that settles on another reef	Success rate of potential disease spread
Self recruitment	Fraction of infectious material settling on a given reef that has been released on the same reef	Potential for disease to settle on a given reef

Table 1. Indicators used to analyze the modeled exchanges of infected material for each considered type of currents and for each simulated month

2.2 Epidemiological modeling

2.2.1 Model equations

The spread of the SCTLD throughout the FRT is simulated using a connectivity-based Kermack-McKendrick SIR model (Brauer, 2008). SIR models are among the most standard epidemiological models. They divide individuals into three compartments: susceptible (S), infectious (I) and removed (R). When affected by the disease, susceptible individuals become infectious and infect other susceptible individuals until they are removed, either by recovery or death. Such models usually rely on the hypothesis of an homogeneous, well-mixed population. To account for the spatial heterogeneity of the FRT, the basic SIR formulation is here modified by considering the proportions of susceptible (S_j), infectious (I_j) and removed (R_j) corals of each polygon reef j. In this epidemiological model, individual reefs interact through the exchange of infectious material as represented by the connectivity matrix. For each sub-reef j and at any time, the following relations hold: $0 \leq S_j, I_j, R_j \leq 1$ and $S_j + I_j + R_j = 1$. The evolution of these proportions through time is governed by the following equations:

$$\frac{dS_j}{dt} = -\beta \sum_i \frac{A_i}{A_j} I_i \tilde{C}_{ij} S_j - \beta'(I_j) S_j I_j$$

$$\frac{dI_j}{dt} = \beta \sum_i \frac{A_i}{A_j} I_i \tilde{C}_{ij} S_j + \beta'(I_j) S_j I_j - \sigma I_j \qquad (2)$$

$$\frac{dR_j}{dt} = \sigma I_j$$

where $\tilde{C}_{ij}$ is the entry of reef (i, j) of the normalized potential connectivity matrix [-], A_i is the area of reef polygon i [km^2], σ is the removal rate [day^{-1}], and β and $\beta'(I_j)$ are the inter- and intra-reef disease transmission rates [day^{-1}], respectively. In this model, infectious corals of reef i can infect corals of reef j if there is non-zero probability of infectious material exchange from reef i to reef j, given by $\tilde{C}_{ij}$. Moreover, to account for coral resistance to the disease, the intra-reef transmission function $\beta'(I_j)$ has the shape of a

186 smooth step function of the proportion of infectious corals I_j and writes:

$$\beta'(I_j) = \frac{\beta'_0}{2}(1 + \tanh[(I_j - I_0)/\tau]), \tag{3}$$

187 where I_0 is a threshold on the infection population above which intra-reef transmission becomes significant,
188 and τ is a measure of the interval over which the transition for low to high transmission occurs. As
189 long as the proportion of infectious corals on reef j is below I_0, the only infection mechanism taking
190 place is connectivity-driven transmission at rate β. Once the threshold is exceeded ($I_j \geq I_0$), intra-reef
191 transmission with rate β'_0 is activated. A larger value of threshold I_0 corresponds to a greater resistance to
192 disease for corals and therefore a slower spread of the disease within reef j. Coral birth and natural (*i.e.*
193 non SCTLD-related) death rates are not taken into account in this model, which amounts to assume that
194 they balance each other. For this study the same values were used for β and β'_0.

2.2.2   Calibration

196   Transmission and removal parameters of σ and β'_0 are fitted to disease prevalence observations averaged
197 over all colonies from 6 permanent monitoring sites in the Lower Keys in order to accurately simulate
198 the temporal evolution of S_j, I_j, R_j on each infected reef polygon. **[Could you provide some details on**
199 **these data prevalence observations ?]** To relate our model framework to the compiled data, Eqs. 2 are
200 simplified to a single-reef SIR model:

$$\frac{dS}{dt} = -\beta'_0 SI$$
$$\frac{dI}{dt} = \beta'_0 SI - \sigma I \tag{4}$$
$$\frac{dR}{dt} = \sigma I$$

201 Due to the low values of the entries in the normalized connectivity matrix $\tilde{C}_{ij}$, intra-reef transmission,
202 when activated, is the dominant infection mechanism of Eqs. 2. Consequently, Eqs. 4 give a reasonable
203 approximation of the evolution of the disease on sub-reefs for which $I_j > I_0$. Using this approximation,
204 the ratio β'_0/σ is imposed by matching the modeled proportion of susceptible corals remaining after the
205 disease has vanished (S_∞) with observations. A standard property of a SIR model solution is that

$$S_\infty - \frac{\sigma}{\beta'_0} \log(S_\infty/S_0) = 1 \tag{5}$$

206 where the initial proportion of susceptible corals (S_0) is taken equal to $1 - I_0$ (see for instance Murray
207 (2007)). In the framework of Eqs. 4, the ratio β'_0/σ gives the value of the basic reproduction number R_0,
208 defined as the average number of secondary cases produced by one infected individual introduced into a
209 population of susceptible individuals (Keeling and Rohani, 2007). This number is used in epidemiological
210 models to determine whether an emerging infectious disease can spread in a population ($R_0 > 1$) or not
211 ($R_0 < 1$). The obtained basic reproduction number is then used to express σ in terms of β'_0 and calibrate its
212 value in order to reproduce as well as possible the temporal evolution of the colonies-averaged susceptible
213 population shown in Fig. 5.

2.2.3   Initialization

215   In order to solve Eqs. 2, initial conditions are needed, *i.e.* proportions of susceptible, infectious and
216 recovered corals at the beginning of the simulated period. This information is constructed based on different
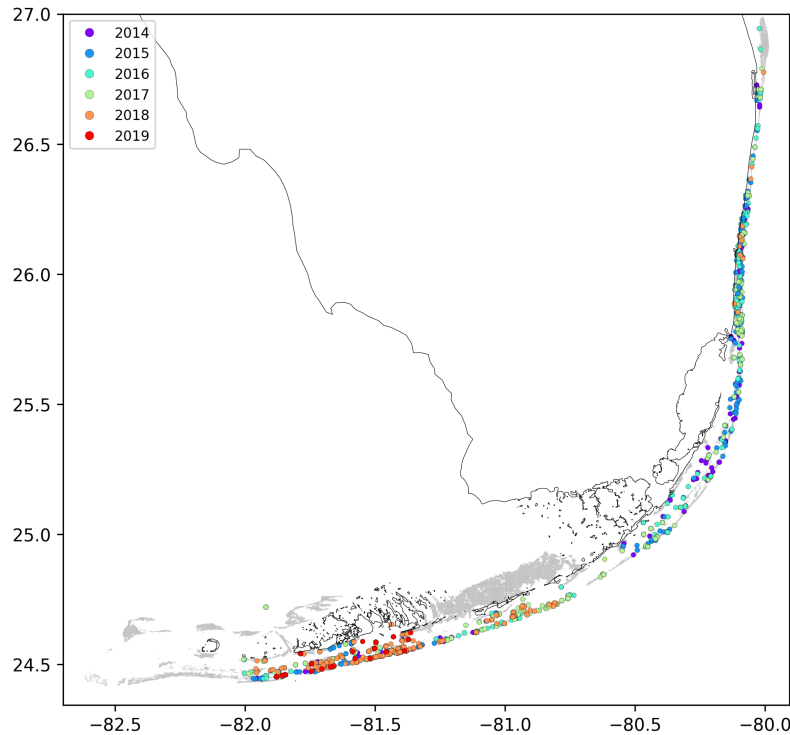
Figure 2. Locations of the disease observations between 2014 and 2019 recorded in the data sets used in this study

field-collected datasets: : (i) Coral Reef Evaluation and Monitoring Project (CREMP; 2014–2017), (ii) CREMP Presence/Absence Data (CREMP P_A; 2016–2017), (iii) Southeast Florida Coral Reef Evaluation and Monitoring Project (SECREMP; 2014– 2017), (iv) Florida Reef Resilience Program Disturbance Response Monitoring (FRRP; 2014–2017), (v) Hurricane Irma Rapid Reef Assessment (IRMA; 2017, Viehman et al. (2018)), (vi) the Southeast Florida Action Network citizen science program (SEAFAN; 2014–2017), and (vii) the Southern Coral Disease Margin field effort (2017; Neely (2018)). These datasets give the locations and dates at which the SCTLD has been observed throughout the FRT. The locations of these observations are shown in Fig. 2. Using this information, we first delineate an infected zone by constructing the concave hull of the points where the disease was observed before May 2018. The reefs infected prior to the beginning of our simulated period are then defined as the reefs located inside the constructed zone. The time of observed infection is then spatially interpolated on each reef of the infected zone by kriging with a Gaussian semivariogram using Python `pyKrige` module. Assuming an initial state $(S, I, R) = (1 - I_0, I_0, 0)$ when the disease was observed, the proportions of susceptible, infectious and removed corals on each reef of the infected zone on the 1st May 2018 is finally approximated using the simplified equations 4. Reefs outside of the infected zone are initialized with a population of 100% of susceptible corals.

2.2.4 Computation of front speed

Muller et al. (2020) estimated the speed of the spreading STCLD epidemics at around 92 m/day in the southern section of the FRT. In order to assess our simulation results in regard to this value, we developed a methodology to compute the displacement of the disease front during a given time interval within our simulated period. First, the concave hull of the infected polygons at the beginning of the time interval H_0 is computed. Then the concave hull of the polygons infected during the time interval H_1 is computed while
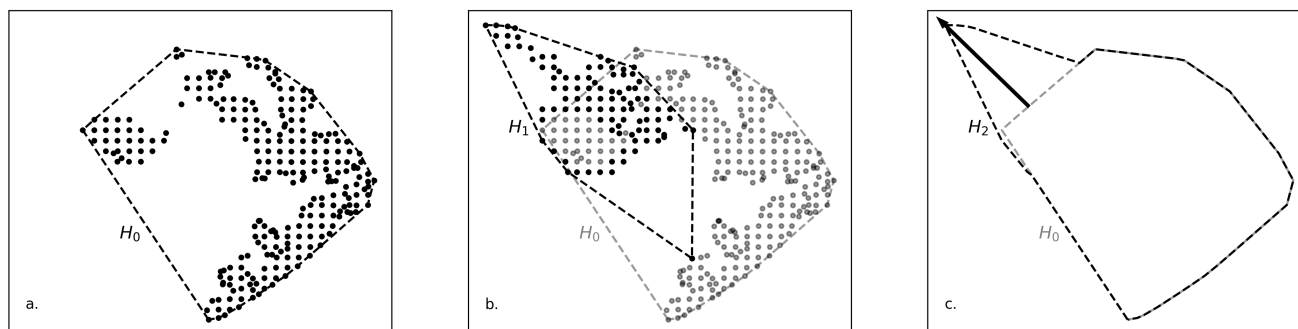
Figure 3. Method used to compute the disease front displacement during a simulated time interval. **a.** Concave hull of the infected polygons at the beginning of the simulated period H_0. **b.** Concave hull of the polygons infected during the simulated simulated H_1. **c.** Arrow showing the computed front displacement during simulated time interval between H_0 and H_2, the union of H_0 and H_1.

239 the concave hull H_2 is defined as the union of H_0 and H_1. This methodology is illustrated in Fig. 3. The
240 distance traveled by the disease front is then obtained by computing the maximum distance between a pair
241 of points of H_0 and H_2. The epidemics front speed is finally computed by dividing the resulting distance
242 by the number of days in the simulated time interval.

243   Permanent Plot data

244 **2.3 Transmission experiments**

245   In parallel to this modeling study, laboratory-based transmission experiments of SCTLD were conducted
246 by several independent groups for various end points including transmission dynamics and samples
247 for molecular and histological analysis. Requests for transmission data were sent to members of the
248 'Transmission' sub group of the Florida Disease Advisory Committee's 'Research' working group as well
249 as any other additional researchers that may have been conducting transmission studies on SCTLD. Data
250 that was requested and subsequently provided included the location, dates, and duration of the experiment,
251 the species used as the diseased colony (donor of disease agents) and apparently healthy colony (exposed
252 to diseased agents), the number of successful transmissions as well as the incubation period following a
253 contact with disease agents prior to disease signs. Additional information included the size of the colonies
254 used in the experiment, the percent tissue loss of the diseased (donor) colony at beginning of the experiment,
255 and whether the apparently healthy (exposed) fragment was touching the diseased colony or not.

256   The average probability of successful disease transmission was determined by taking the mean of the
257 number of colonies exposed to the disease in each study divided by the total number of coral colonies
258 exposed to diseased colonies. The 'incubation' period was identified as the average number of days after an
259 apparently healthy coral colony was exposed to a diseased colony before visual disease signs occurred (i.e.,
260 active tissue loss). Only corals that eventually showed disease signs were integrated within the incubation
261 period calculation.

262   Data was provided from 8 different research groups representing 15 institutions and 19 total collaborators
263 providing a total of 109 data points. After amalgamating the contributed data, the mean probability of
264 transmission of SCTLD to an apparently healthy coral had a likelihood of approximately 44.8 ± 3.6 %.
265 The probability of transmission ranged from 0 to 100% depending on the experiment. Additionally, the
266 time between exposure of an apparently healthy coral to a diseased coral and subsequently showing initial
267 signs of tissue loss (i.e., incubation period) was 9.7 ± 1 days.

3 RESULTS

3.1 Exchanges of infected materials

268

269   Among the three modes of transport, bottom currents exhibited the lowest range as they generate the
270   networks with the smallest weighted connectivity length (Fig. 4). However, infectious matters transported
271   by bottom currents have the largest settlement success rate as these currents generate the graphs with the
272   largest fraction exchanged. Therefore, bottom currents tend to transport more infectious material on closer
273   reefs compared to the two other modes of transport.

274   Mean and surface currents, on the other hand showed similar spreading ranges with mean WCL of 20.63
275   km and 21.39 km respectively. However, the infectious matters that surface currents transport have the
276   weakest probability to successfully settle on reefs. Consequently, surface currents and bottom currents
277   produce networks with similar mean out-degree, although surface currents have the potential to transport
278   infectious matter on more reefs. Nonetheless, networks have larger median out-degree with bottom currents
279   than with surface currents, which suggests that surface currents have a lower spreading potential than
280   bottom currents. As a result of their large WCL and fraction exchanged, barotropic currents on the other
281   hand exhibit the largest mean out-degree, which suggest that they have a strong dispersal potential.

282   Self recruitment gives the proportion of infectious material settling on a reef that was produced on the
283   same reef. The greater its values, the more the reef is isolated from the rest of the network. Since infectious
284   material is less likely to settle on isolated reefs, self recruitment measures the probability for the disease to
285   settle on a given reef, whereas all three other indicators inform on the reef spreading potential. Fig. 4 shows
286   that the disease is more likely to settle on the reefs of networks generated by mean currents. This result is
287   consistent with the values of the other connectivity measures, as reefs tend to be more strongly connected
288   with mean currents. On the other hand, reefs are more isolated with bottom currents, as they produce the
289   graphs with lowest WCL and out-degree. Finally, surface currents generate larger self recruitment values
290   than mean currents as they exhibit the lowest fraction exchanged.

3.2 Epidemiological model results

291

292   Best fit to averaged disease prevalence observations is obtained with transmission rate $\beta_0^{-1\prime} = 6.45$ days
293   and removal rate $\sigma^{-1} = 6.99$ days. Comparison of the evolution of the state described by Eqs 4 results
294   with observations is shown in figure 5. Our model results accurately reproduce the observed fraction of
295   susceptible individuals on colonies through time. However, the modeled fraction of removed individuals
296   overestimates observations by about 5%. These discrepancies might be explained by the presence of
297   "Unknown" values in our data sets as well as the simplifying assumptions of SIR models. Transmission
298   and removal rates are found to have fairly close values with basic $\beta_0^\prime/\sigma$ being equal to 1.0345. This
299   proximity in rate values is imposed by Eq. 5, as aggregated observations show a proportion of susceptible
300   individuals of about 85% at the end of the outbreak. Since infection and removal occur at very close rates,
301   the instantaneous proportion of infectious individuals on the reefs remains low through the outbreak, with
302   a maximum value of about 0.4%.

303   Using the above calibrated epidemiological parameters, epidemiological model simulations were
304   performed from 1st May 2018 to 1st April 2019 for each type of currents and different values of the
305   infection threshold I_0. A summary of the simulation results are shown in Fig. 6. Two metrics were
306   used to assess the accuracy of the model. First, the modeled front speed was compared to the reference
307   rate of 92 m/day derived by Muller et al. (2020). Furthermore, we computed the mean of the distances
308   between each point where SCTLD had been observed during our simulated period and the centroid of
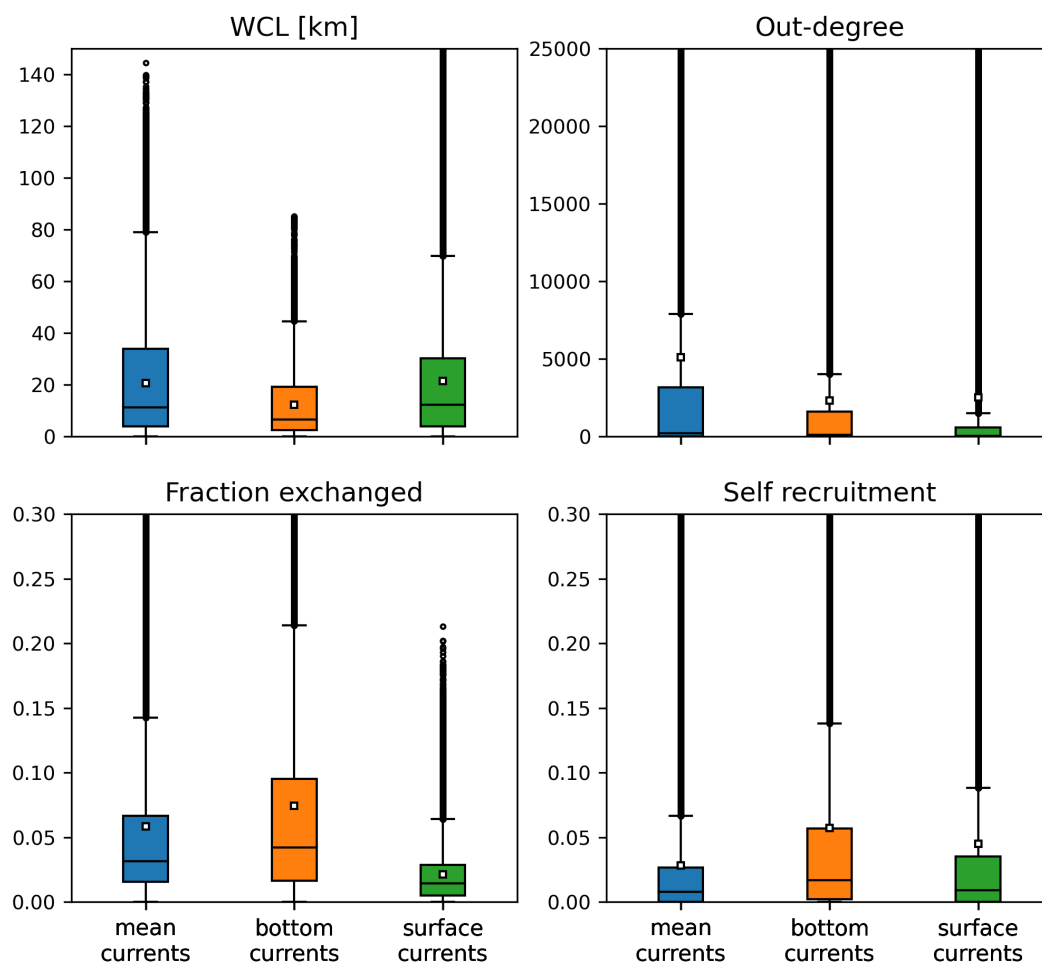
Figure 4. Distribution of the indicators derived from the monthly connectivity matrices computed for each type of current during our simulated period. Mean values are indicated by white squares

309   the closest reef polygon predicted to be infected by our model during the same period. Bottom currents
310   produced the slowest modeled disease propagation with a maximum front speed of ~ 20 m/day, while
311   simulations performed with surface currents spread the disease at a maximum speed of of about 60 m/day.
312   However, surface currents tend to propagate the disease to the north, rather than westward, along the
313   Florida Keys. This explains why bottom currents predict disease occurrance closer to field observations
314   despite exhibiting slower front speed. Finally, Mean barotropic currents outperform other types of current
315   predictions regarding both criteria with a front speed of 107 m/day and a mean geographical accuracy of
316   ~ 1.2 km. This suggests that the disease agents of SCTLD may be transported within neutrally buoyant
317   material driven from reef to reef inside the water column by mean currents.

318   Moreover, Fig. 6 shows a strong dependence of model results to infection threshold I_0, that gives
319   the proportion of infectious individual that colonies can withstand before exponential disease growth is
320   triggered on reef. Front speeds of both mean and bottom currents reach a plateau for values of infection
321   threshold between $I_0 = 0.05\%$ and $I_0 = 0.1\%$, while the minimal prediction error is attained around
322   $I_0 \approx 0.078\%$ with mean currents. For $I_0 > 0.1\%$, intra-reef infection is strongly impeded and populations
323   of infectious individuals on infected reefs are not able to become sufficiently large to infect other colonies
324   on reefs they are connected to. For values of I_0 lower than 0.05% on the other hand, intra-reef infection
325   dominates and coral population on infected reefs is removed too fast to efficiently spread the disease
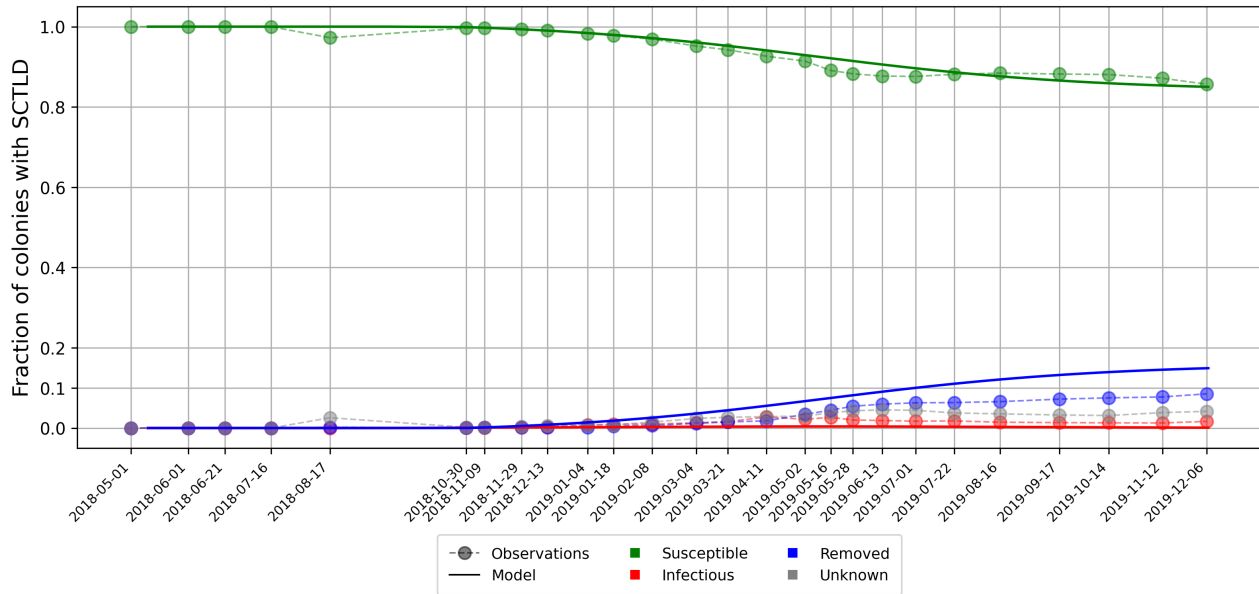
Figure 5. Disease prevalence averaged over all monitored sites over time as modeled by Eqs. 4 using calibrated transmission and removal parameters $\beta_0^{-1\prime} = 6.45$ days and $\sigma^{-1} = 6.99$ days.

326 through the network. Since disease propagation throughout the FRT only occurs for fairly small values of
327 I_0 in our model, corals are expected to have low resistance to the causative agent of the SCTLD.

328   The results shown in Fig. 6 were obtained by removing the large reef located North to Vaca key, denoted
329 Vaca reef in Frys et al. (2020), from our reef polygons. Preliminary simulations showed that this reef
330 has close to no impact on the modeled spread of the disease to the rest of the FRT, as it sends very little
331 infectious material to southerly and easterly neighboring reefs. Moreover, Vaca reef has a low coral coverage
332 $(0 - 10\%)$, which strongly impedes disease spread on the reef. However, as coral coverage is not taken into
333 account in our epidemiological model, propagation of the disease on the reef was overestimated. This led
334 to unrealistically strong modeled front speed variations due to the large size of the reef. Consequently, and
335 in the absence of SCTLD observations on Vaca reef, it has been removed from our reef polygons in order
336 to avoid overestimating the front speed.

4 DISCUSSION AND CONCLUSIONS

337 We have developed an epidemio-hydrodynamic model to simulate the spread of the SCTLD through
338 the entire FRT. Calibrating our model with colonies-averaged prevalence observations, we estimate the
339 species-averaged reproduction number R_0 to be barely larger than one. Our model simulations suggest
340 that only the barotropic currents are able to reproduce the observed spread of the disease. Bottom current
341 do not spread infectious material far enough while surface currents do not allow infectious material to
342 spend enough time over the reefs to strongly infect them. The causative agent of the SCTLD is therefore
343 expected to be transported within neutrally buoyant particles inside the water column. With this mode of
344 transport, the propagation of the disease from reef to reef only occurs for a well-defined range of values of
345 the infection threshold I_0. This threshold is defined as the proportion of colonies that have to be infected
346 to trigger a rapid spread of the disease over the entire reef. Our result suggest that this occurs as soon as
347 $0.05 - 0.1\%$ of colonies are infected. On average, corals are thus expected to a have low resistance to the
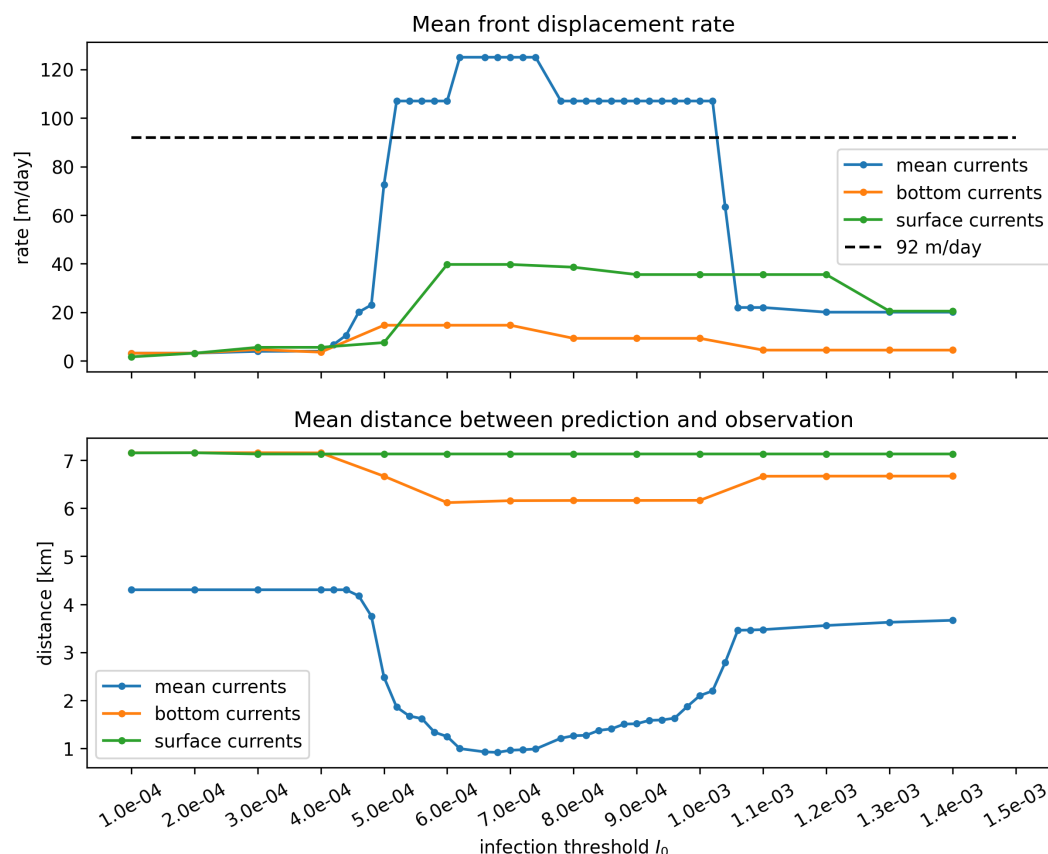348 SCTLD.

Figure 6. Summary of epidemiological model simulations with calibrated transmission parameters. **Top:** Modeled disease front speed for each type of current with respect to intra-reef infection threshold I_0. **Bottom:** Mean distance between predicted infected reefs and observed disease points. These results show that mean barotropic currents outperform other modes of transport at reproducing the observed spread of the disease. The appearance of a plateau suggests that model predictions are very sensitive to the value of the infection threshold I_0.

After calibration, we estimated the species-averaged basic reproduction number β'_0/σ to be equal to 1.0835. This value being close to 1, modeled infectious individuals are removed from the system almost as fast as susceptible individuals get infected. This causes the proportion of infectious corals on the reefs to remain pretty low (*i.e.* $\leq 0.4\%$) through time. This suggests that only a small fraction of the colony causes the disease to spread on the reef during the outbreak. The observation-based species-averaged transmission period of 6.45 days used in this model seems to be a reasonable estimation of the disease transmission dynamics as it is of the same order of magnitude as the experimentally-derived mean incubation period of 9.7 days. The difference between the two values can be explained by field measurement uncertainties as well as the inability to perfectly mimic field conditions in laboratory. In this study, the same values were used for inter- and intra-reef rates β and β'_0. This implies that the infectiousness of the causative agent is not reduced during its journey from reef to reef. However, to assess the impact of this assumption, epidemiological model simulations were performed with $\beta = \beta'_0/2$. The resulting disease front speeds did not exceed 20 m/day. This strong decrease can be explained by the interplay between inter- and intra-reef infection. Reducing inter-reef transmission rates decreases the proportion of infectious corals on reefs attained by infectious materials, which in turn reduces the amount of infectious matter sent to the rest of the network. This suggests that, to reproduce the observed spread, inter- and intra-reef transmission rates

365 must have similar magnitude, *i.e.* that the causative agent is almost not degraded while traveling from reef
366 to reef. **Is this consistent with Rhodobacterales and Rhizobiales ?**

367   The fact that mean barotropic currents outperform the other modes of transport can be explained by
368 considering the trajectories of the particles used to model the transport of the vector of the disease causative
369 agent. Due to the impact of winds on positively buoyant materials, particles driven by surface currents
370 are likely to be blown away from the reefs. Moreover, even when winds are pushing particles along the
371 reef line, these particles spend less time over the same region than particles driven by mean and bottom
372 currents. Smaller amounts of particle mass will therefore settle on reef polygons, leading to lower entries
373 of the potential connectivity matrix, *i.e.* lower exchange of infectious material between reefs. Hence,
374 despite being able to transport the disease over greater distances, surface currents are less likely to drive
375 the propagation of the disease. Particles driven by bottom currents, on the other hand, remain longer over
376 the same region, producing larger entries of the potential connectivity matrix. Due to these large exchange
377 probabilities between reefs, bottom currents are better at propagating the disease (Fig. 6). Nevertheless,
378 bottom currents being relatively slower, exchanges of infected materials occur on a limited geographical
379 range. Mean barotropic currents, that carry particles on greater distances while allowing for sufficiently
380 large amounts of infected mass to settle on reef polygons, are thus best suited to propagate the disease (Fig.
381 6).

382   Since mean currents are the only mode of transport that successfully reproduces the observed propagation
383 speed of the disease in our model, the disease causative agent is expected to be transported within neutrally
384 buoyant material inside the water column. Current-driven propagation seems reasonable as water-borne
385 transmission is implicated as an important spreading mechanism for multiple coral diseases, including
386 white band disease, white plague disease, white pox disease, white syndrome disease, *Porites* ulcerative
387 white spots diseases, skeletal eroding band disease (Shore and Caldwell, 2019). **[examples of neutrally**
388 **buoyant vectors ? mucus ?]**. The causative agent might also be transported within fine sediments such
389 as silt, as suggested by Rosales et al. (2020). Such sediments are easily eroded in shallow areas around
390 coral reefs and would therefore be mostly transported inside the water column by mean barotropic currents.
391 This hypothesis might be tested by adapting the deposition rate γ used in our experiments to be consistent
392 with the sedimentation rate of silt. However, such modification of γ would alter the entries of our potential
393 connectivity matrices. Nonetheless, the sensitivity of the connectivity matrices to the value of γ has been
394 briefly assessed by generating new matrices using particles with a half-life of 15 days (γ increased by a
395 factor two). Although these matrices exhibited stronger short-range connectivity, the impact on connectivity
396 indicator values remained limited ($< 10\%$). This suggests that the main results of this study would remain
397 valid for fine sediments.

398   Coral resistance to the SCTLD in represented by parameter I_0, defined as the maximum proportion
399 of the colony that can get infected without causing the disease to spread to the rest of the colony. The
400 plateau shown in Fig. 6 highlights the impact of this parameter on the modeled propagation of the disease.
401 On the one hand, when corals are strongly susceptible to the disease, infectious individuals are removed
402 from the system too fast to become sustainable sources of infectious materials in the network. On the
403 other hand, if corals are weakly susceptible to the disease, very few corals get infected and the disease
404 barely propagates. Our simulations suggest that this value must be fairly low (around 0.01%) in order to
405 successfully spread the disease throughout the FRT. **This seems to imply that susceptible coral species**
406 **have very weak defense mechanisms against the causative agent of the disease. (?)**.
407

408   As with any modeling study, it is important to understand the assumptions on which the model is based.
409 Here, we have used a 2D barotropic ocean model coupled with the 3D model HYCOM (Chassignet et al.,
410 2007) in order to indirectly represent baroclinic phenomena. Such model is well suited to simulate the fate
411 of neutrally-buoyant matters in shallow regions. However, as depth-averaged currents do not accurately
412 approximate the motion of particles in the bottom and surface layers, SLIM velocities have therefore been
413 modified to simulate the exchanges of negatively and positively buoyant matters. Surface current response
414 to wind parameterization is based on the results of Ardhuin et al. (2009), consistent with observations. In
415 this study, measured surface currents are shown to be in the order of $1.0\% - 1.8\%$ of the wind speed, in a
416 direction $10° - 40°$ to the right of the wind. Moreover, the norm and veering angle used to parameterize
417 bottom currents are expected to be reasonably accurate approximations as they are consistent with both
418 Ekman theory and current observations in the Forida Keys (Perlin et al., 2007; Kundu, 1976; Smith, 2009).
419 Although such estimation of surface and bottom currents is disputable, using a 2D model allows for
420 reef-scale resolution throughout the whole FRT. Such high-resolution allows to capture recirculation eddies
421 around islands and reefs, that significantly impact the weighted connectivity length as well as the local
422 retention on the reefs.

423   The appearance of an interval of optimal values of threshold I_0 for the propagation of the disease in our
424 results highlights the impact of coral resistance on the spread of SCTLD through the FRT. Therefore, a
425 further step in our modeling approach would be further dividing coral populations of our polygons into
426 highly susceptible (*e.g. Dichocoenia stokesii*, *Meandrina meandrites*), intermediately susceptible (*e.g.*
427 *Orbicella faveolata*, *Montastrea cavernosa*), and weakly susceptible (*e.g. Acropora Palmata*, *Acropora*
428 *cervicornis*) sub-populations. The proportions susceptible, infectious and removed individuals within these
429 sub-populations would then be modeled with specific transmission (β, β_0') and removal (σ) rates as well as
430 specific infection thresholds I_0. Such approach would however require a fine knowledge of the distribution
431 of the different coral species throughout the FRT. This knowledge about coral coverage could also be used
432 to avoid overestimation of the front propagation, as in the case of Vaca reef.

433   Despite the limitations of its current formulation, we believe that our model brings unprecedented
434 perspectives on the propagation mechanism of the SCTLD through the FRT. Using a reef-scale spatial
435 resolution, we determined the most probable mode of transport for the vector of the disease agent and
436 deduced its species-averaged reproduction number based on prevalence observations. Besides, our model
437 formulation provides a framework to quantity coral resistance to the disease. As our model results are
438 continuous through time, they can exhibit the variability of the propagation of the SCTLD through time
439 and therefore bring additional insight to observation data. This study therefore provides much-needed
440 complementary insight on the identification of the causative agent of the Stony Coral Tissue Loss disease
441 and the management of the crisis it generates. Furthermore, our modeling approach could be applied to
442 other affected areas of the Caribbean, where there is still time to perform active management of the disease.

CONFLICT OF INTEREST STATEMENT

443 The authors declare that the research was conducted in the absence of any commercial or financial
444 relationships that could be construed as a potential conflict of interest.

AUTHOR CONTRIBUTIONS

FUNDING

ACKNOWLEDGMENTS

REFERENCES

Aeby, G., Ushijima, B., Campbell, J. E., Jones, S., Williams, G., Meyer, J. L., et al. (2019). Pathogenesis of a tissue loss disease affecting multiple species of corals along the florida reef tract. *Frontiers in Marine Science* 6, 678

Alvarez-Filip, L., Estrada-Saldívar, N., Pérez-Cervantes, E., Molina-Hernández, A., and González-Barrios, F. J. (2019). A rapid spread of the stony coral tissue loss disease outbreak in the Mexican Caribbean. *PeerJ* 7, e8069

Ardhuin, F., Marié, L., Rascle, N., Forget, P., and Roland, A. (2009). Observation and estimation of Lagrangian, Stokes, and Eulerian currents induced by wind and waves at the sea surface. *Journal of Physical Oceanography* 39, 2820–2838

Aronson, R. B. and Precht, W. F. (2001). White-band disease and the changing face of Caribbean coral reefs. In *The ecology and etiology of newly emerging marine diseases* (Springer). 25–38

Aronson, R. B. and Precht, W. F. (2006). Conservation, precaution, and Caribbean reefs. *Coral reefs* 25, 441–450

Bidegain, G., Powell, E., Klinck, J., Ben-Horin, T., and Hofmann, E. (2016a). Microparasitic disease dynamics in benthic suspension feeders: infective dose, non-focal hosts, and particle diffusion. *Ecological modelling* 328, 44–61

Bidegain, G., Powell, E. N., Klinck, J. M., Ben-Horin, T., and Hofmann, E. E. (2016b). Marine infectious disease dynamics and outbreak thresholds: contact transmission, pandemic infection, and the potential role of filter feeders. *Ecosphere* 7, e01286

Blondeau, J., Brandt, M., Donovan, C., Eakin, M., Edwards, K., Edwards, K., et al. (2020). Coral reef condition: A status report for the US Virgin Islands

Brandt, M. E. and McManus, J. W. (2009). Dynamics and impact of the coral disease white plague: insights from a simulation model. *Diseases of aquatic organisms* 87, 117–133

Brauer, F. (2008). Compartmental models in epidemiology. In *Mathematical epidemiology* (Springer). 19–79

Burgess, S. C., Kingsford, M. J., and Black, K. P. (2007). Influence of tidal eddies and wind on the distribution of presettlement fishes around One Tree Island, Great Barrier Reef. *Marine Ecology Progress Series* 341, 233–242

Chassignet, E. P., Hurlburt, H. E., Smedstad, O. M., Halliwell, G. R., Hogan, P. J., Wallcraft, A. J., et al. (2007). The HYCOM (hybrid coordinate ocean model) data assimilative system. *Journal of Marine Systems* 65, 60–83

Dustan, P. and Halas, J. C. (1987). Changes in the reef-coral community of Carysfort Reef, Key Largo, Florida: 1974 to 1982. *Coral Reefs* 6, 91–106

483 Figueiredo, J., Baird, A. H., and Connolly, S. R. (2013). Synthesizing larval competence dynamics and
484   reef-scale retention reveals a high potential for self-recruitment in corals. *Ecology* 94, 650–659

485 Frys, F., Saint-Amand, A., Le Hénaff, M., Figueiredo, J., Kuba, A., Walker, B., et al. (2020). Fine-scale
486   coral connectivity pathways in the Florida Reef Tract: Implications for conservation and restoration.
487   *Frontiers in Marine Science* in press. doi:10.3389/fmars.2020.00312

488 FWC, F. (2017). Unified reef map v2. 0

489 Gardner, T. A., Côté, I. M., Gill, J. A., Grant, A., and Watkinson, A. R. (2003). Long-term region-wide
490   declines in Caribbean corals. *science* 301, 958–960

491 Geuzaine, C. and Remacle, J.-F. (2009). Gmsh: A 3-d finite element mesh generator with built-in pre-and
492   post-processing facilities. *International journal for numerical methods in engineering* 79, 1309–1331

493 Harvell, D., Jordán-Dahlgren, E., Merkel, S., Rosenberg, E., Raymundo, L., Smith, G., et al. (2007). Coral
494   disease, environmental drivers, and the balance between coral and microbial associates. *Oceanography*
495   20, 172–195

496 Keeling, M. and Rohani, P. (2007). Stochastic dynamics. *Modeling Infectious Diseases in Humans and*
497   *Animals* , 190–230

498 Kourafalou, V. H. and Kang, H. (2012). Florida current meandering and evolution of cyclonic eddies along
499   the Florida Keys Reef Tract: Are they interconnected? *Journal of Geophysical Research: Oceans* 117

500 [Dataset] Kramer, P., Roth, L., and Lang, J. (2019). Map of stony coral tissue loss disease outbreak in the
501   Caribbean. www.agrra.org. ArcGis Online. (accessed June 12, 2020)

502 Kuffner, I. B., Lidz, B. H., Hudson, J. H., and Anderson, J. S. (2015). A century of ocean warming on
503   florida keys coral reefs: historic in situ observations. *Estuaries and Coasts* 38, 1085–1096

504 Kundu, P. K. (1976). Ekman veering observed near the ocean bottom. *Journal of Physical Oceanography*
505   6, 238–242

506 Kuta, K. and Richardson, L. (1996). Abundance and distribution of black band disease on coral reefs in the
507   northern Florida Keys. *Coral reefs* 15, 219–223

508 Lambrechts, J., Hanert, E., Deleersnijder, E., Bernard, P.-E., Legat, V., Remacle, J.-F., et al. (2008). A
509   multi-scale model of the hydrodynamics of the whole Great Barrier Reef. *Estuarine, Coastal and Shelf*
510   *Science* 79, 143–151

511 Manzello, D. P. (2015). Rapid recent warming of coral reefs in the Florida Keys. *Scientific reports* 5,
512   16762

513 Miller, J., Muller, E., Rogers, C., Waara, R., Atkinson, A., Whelan, K., et al. (2009). Coral disease
514   following massive bleaching in 2005 causes 60% decline in coral cover on reefs in the US Virgin Islands.
515   *Coral Reefs* 28, 925

516 Muller, E. M., Sartor, C., Alcaraz, N. I., and van Woesik, R. (2020). Spatial epidemiology of the
517   Stony-Coral-Tissue-Loss Disease in Florida. *Frontiers in Marine Science* 7, 163

518 Murray, J. D. (2007). *Mathematical biology: I. An introduction*, vol. 17 (Springer Science & Business
519   Media)

520 Neely, K. (2018). Surveying the Florida Keys southern coral disease boundary. *Florida DEP. Miami, FL* ,
521   1–15

522 [Dataset] NOAA (2018). Stony Coral Tissue Loss Disease Case Definition. . Available online at:
523   `https://nmsfloridakeys.blob.core.windows.net/floridakeys-prod/media/`
524   `docs/20181002-stony-coral-tissue-loss-disease-case-definition.pdf`
525   (accessed June 4, 2020)

526 Perlin, A., Moum, J., Klymak, J., Levine, M., Boyd, T., and Kosro, P. (2007). Organization of stratification,
527   turbulence, and veering in bottom Ekman layers. *Journal of Geophysical Research: Oceans* 112

528 Porter, J. W. and Meier, O. W. (1992). Quantification of loss and change in floridian reef coral populations.
529   *American Zoologist* 32, 625–640

530 Precht, W. F., Gintert, B. E., Robbart, M. L., Fura, R., and Van Woesik, R. (2016). Unprecedented
531   disease-related coral mortality in southeastern florida. *Scientific Reports* 6, 1–11

532 Richardson, L. L., Goldberg, W. M., Kuta, K. G., Aronson, R. B., Smith, G. W., Ritchie, K. B., et al. (1998).
533   Florida's mystery coral-killer identified. *Nature* 392, 557–558

534 Rosales, S. M., Clark, A. S., Huebner, L. K., Ruzicka, R. R., and Muller, E. (2020). Rhodobacterales and
535   Rhizobiales are associated with stony coral tissue loss disease and its suspected sources of transmission.
536   *Frontiers in Microbiology* 11, 681

537 Ruzicka, R., Colella, M., Porter, J., Morrison, J., Kidney, J., Brinkhuis, V., et al. (2013). Temporal changes
538   in benthic assemblages on florida keys reefs 11 years after the 1997/1998 el niño. *Marine Ecology*
539   *Progress Series* 489, 125–141

540 Shore, A. and Caldwell, J. M. (2019). Modes of coral disease transmission: How do diseases spread
541   between individuals and among populations? *Marine biology* 166, 45

542 Smith, N. P. (2009). The influence of wind forcing on across-shelf transport in the Florida Keys. *Continental*
543   *Shelf Research* 29, 362–370

544 Sokolow, S. (2009). Effects of a changing climate on the dynamics of coral infectious disease: a review of
545   the evidence. *Diseases of Aquatic Organisms* 87, 5–18

546 Sponaugle, S., Paris, C., Walter, K., Kourafalou, V., and Alessandro, E. (2012). Observed and modeled
547   larval settlement of a reef fish to the Florida Keys. *Marine Ecology Progress Series* 453, 201–212

548 Sutherland, K. P., Porter, J. W., and Torres, C. (2004). Disease and immunity in Caribbean and Indo-Pacific
549   zooxanthellate corals. *Marine Ecology Progress Series* 266, 273–302

550 Team, A. B. R. (2005). Atlantic Acropora status review document. *Report to National Marine Fisheries*
551   *Service* , 152

552 Thomas, C. J., Bridge, T. C., Figueiredo, J., Deleersnijder, E., and Hanert, E. (2015). Connectivity between
553   submerged and near-sea-surface coral reefs: Can submerged reef populations act as refuges? *Diversity*
554   *and Distributions* 21, 1254–1266

555 Thomas, C. J., Lambrechts, J., Wolanski, E., Traag, V. A., Blondel, V. D., Deleersnijder, E., et al. (2014).
556   Numerical modelling and graph theory tools to study ecological connectivity in the Great Barrier Reef.
557   *Ecological Modelling* 272, 160–174

558 Vaz, A. C., Paris, C. B., Olascoaga, M. J., Kourafalou, V. H., Kang, H., and Reed, J. K. (2016). The perfect
559   storm: match-mismatch of bio-physical events drives larval reef fish connectivity between Pulley Ridge
560   mesophotic reef and the Florida Keys. *Continental Shelf Research* 125, 136–146

561 Viehman, S., Gittings, S., Groves, S., Moore, J., Moore, T., and Stein, J. (2018). NCCOS Assessment: Coral
562   Disturbance Response Monitoring (DRM) Along the Florida Reef Tract Following Hurricane Irma From
563   2017-10-09 to 2017- 10-18 (NCEI Accession 0179071). *NOAA National Centers for Environmental*
564   *Information* . Silver Spring, MD: National Centers for Coastal Ocean Science. Available online at:
565   `https://doi.org/10.25921/sscd-6h41`

566 Wolanski, E. (1994). *Physical oceanographic processes of the Great Barrier Reef* (CRC Press)

TABLES AND FIGURES